Electronic Supplementary Material (ESI) for Dalton Transactions.

Electronic Supporting Information

Synthesis and Coordination Behaviour of Aluminate-based Quinolyl Ligands

Jessica E. Waters,[a] Schirin Hanf,[b] Marina Rincón-Nocito,[a] Andrew D. Bond,[a] Raul García-Rodríguez,[c] Dominic S. Wright,[a,*] Annie L. Colebatch[d,*]

[a] *Yusuf Hamied Department of Chemistry, University of Cambridge, Lensfield Road, Cambridge, CB2 1EW, U.K.*

[b] *Karlsruhe Institut für Technologie (KIT), 76131 Karlsruhe, Baden-Württemberg, Germany*

[c] *GIR MIOMeT-IU Cinquima-Química Inorgánica Facultad de Ciencias, Universidad de Valladolid, Campus Miguel, Delibes, 47011 Valladolid, Spain.*

[d] *Research School of Chemistry, Australian National University, Canberra, ACT, 2601, Australia*

Table of Contents

1. Experimental Spectra

1.1 NMR spectra of [(1)Li(μ-X)Li(THF)$_3$] and [{1Li}$_2$(μ-Br)]$^-$Li(THF)$_4^+$ mixture

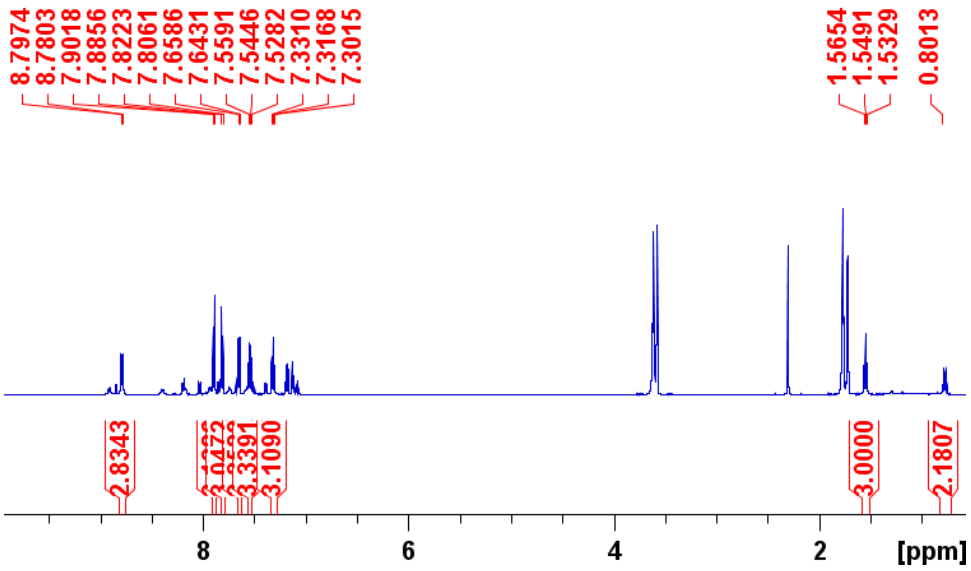

Figure S1:^{1}H NMR spectrum (25 °C, 400 MHz, D$_8$-THF) of [(**1**)Li(μ-X)Li(THF)$_3$] and [{**1**Li}$_2$(μ-Br)]$^-$ Li(THF)$_4^+$ mixture (crystalline sample isolated from reaction).

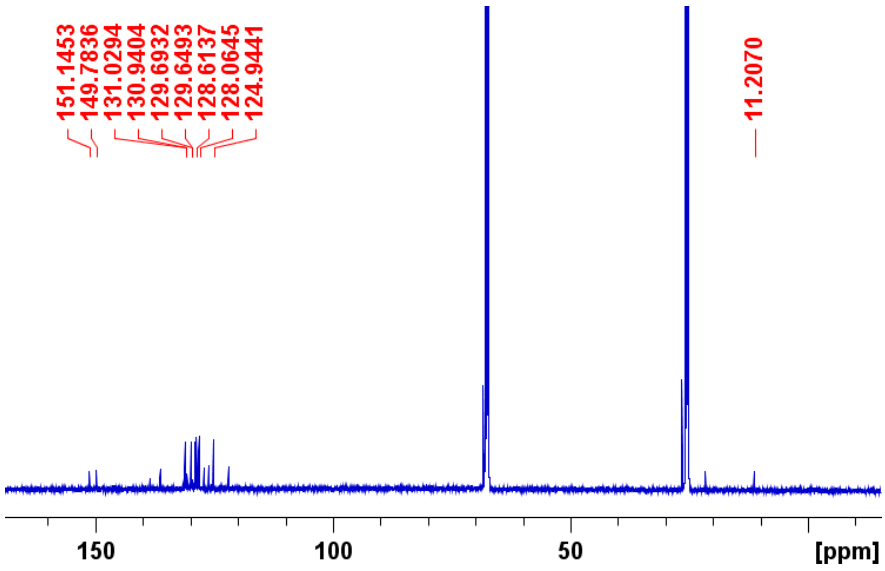

Figure S2: ^{13}C{^{1}H} NMR spectrum (25 °C, 126 MHz, D$_8$-THF) of [(**1**)Li(μ-X)Li(THF)$_3$] and [{**1**Li}$_2$(μ-Br)]$^-$ Li(THF)$_4^+$ mixture (crystalline sample isolated from reaction).

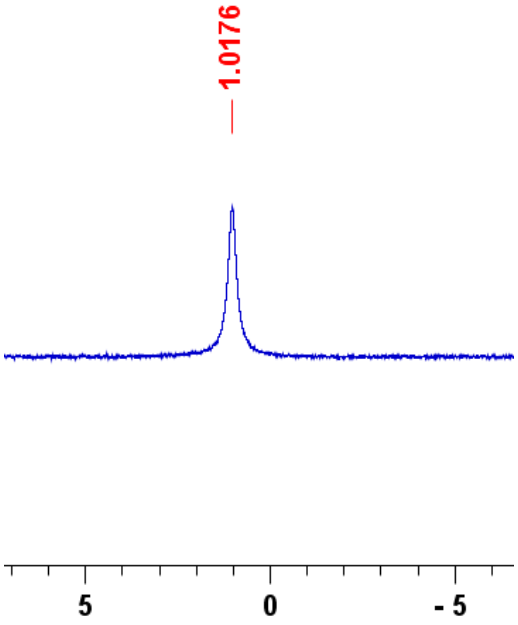

Figure S3: ^{7}Li NMR spectrum (25 °C, 194 MHz, D_8-THF) of [(**1**)Li(μ-Xl)Li(THF)$_3$] and [{**1**Li}$_2$(μ-Br)]$^-$ Li(THF)$_4^+$ mixture (crystalline sample isolated from reaction).

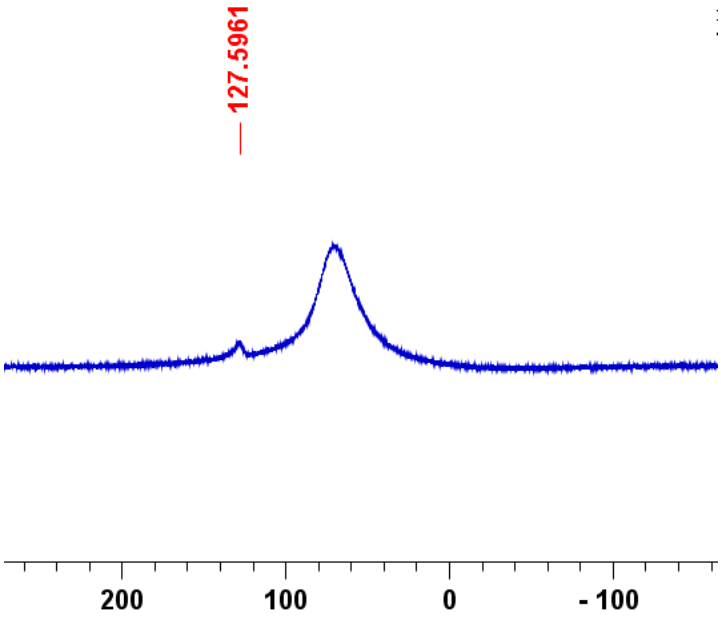

Figure S4: ^{27}Al NMR spectrum (25 °C, 130 MHz, D_8-THF) of [(**1**)Li(μ-X)Li(THF)$_3$] and [{**1**Li}$_2$(μ-Br)]$^-$ Li(THF)$_4^+$ mixture (crystalline sample isolated from reaction).

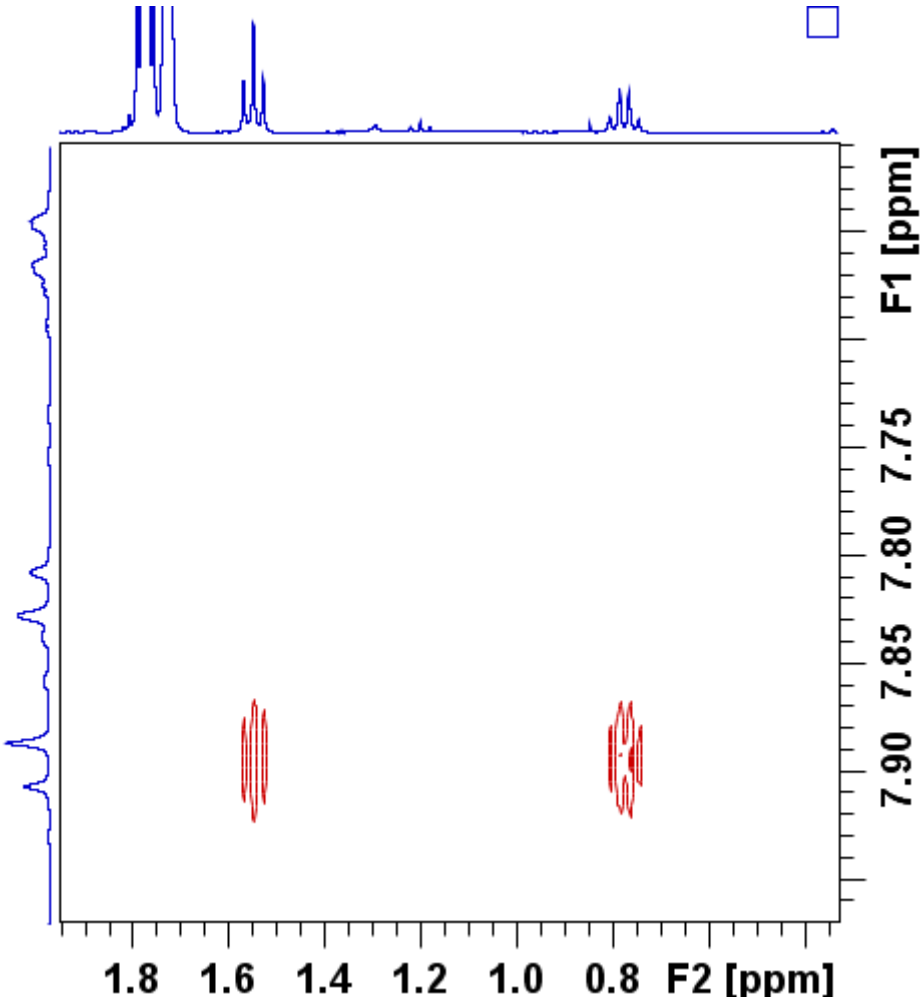

Figure S5: ^{1}H-^{1}H NOESY NMR spectrum (25 °C, 400 MHz, D_8-THF) of [(**1**)Li(μ-X)Li(THF)$_3$] and [{**1**Li}$_2$(μ-Br)]$^{-}$Li(THF)$_4^{+}$ mixture (crystalline sample isolated from reaction).

1.2 NMR spectra of [{EtAl(2-Me-8-qy)$_3$}Li], [(2)Li]

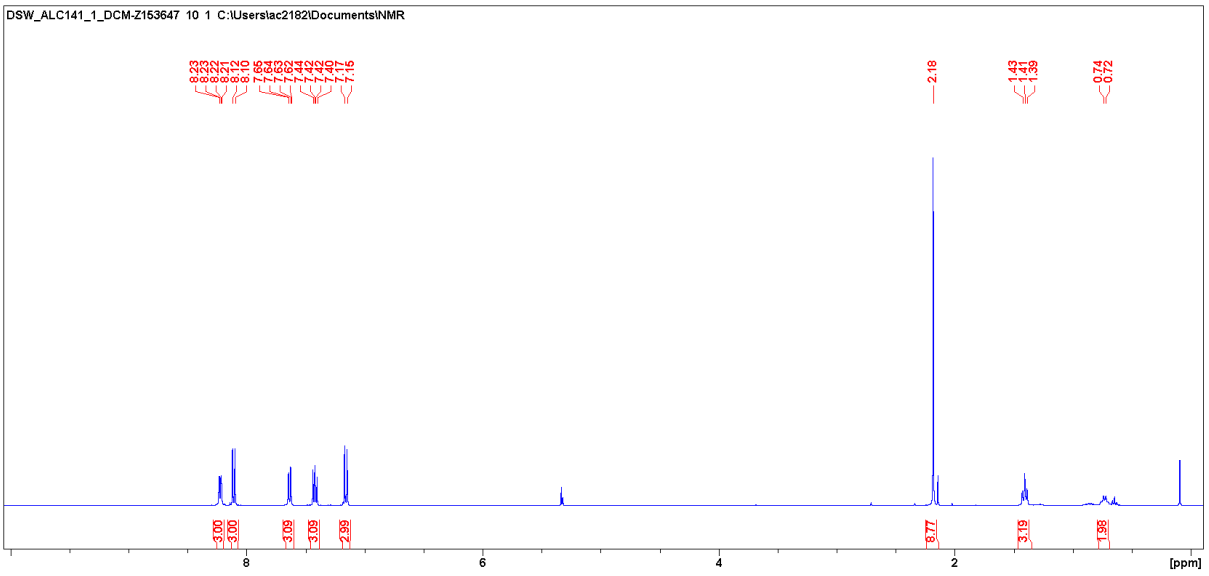

Figure S6: ^{1}H NMR spectrum (25 °C, 400 MHz, CD_2Cl_2) of [{EtAl(2-Me-8-qy)$_3$}Li], [(**2**)Li].

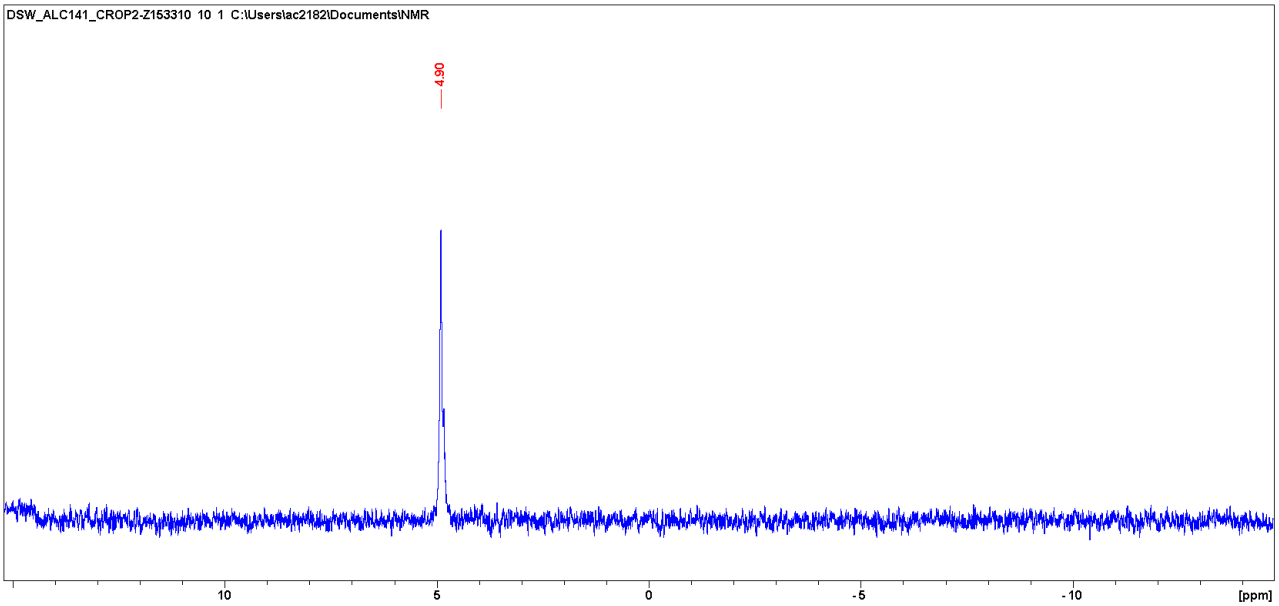

Figure S7: ^{7}Li NMR spectrum (25 °C, 155 MHz, CD_2Cl_2) of [{EtAl(2-Me-8-qy)$_3$}Li], [(**2**)Li].

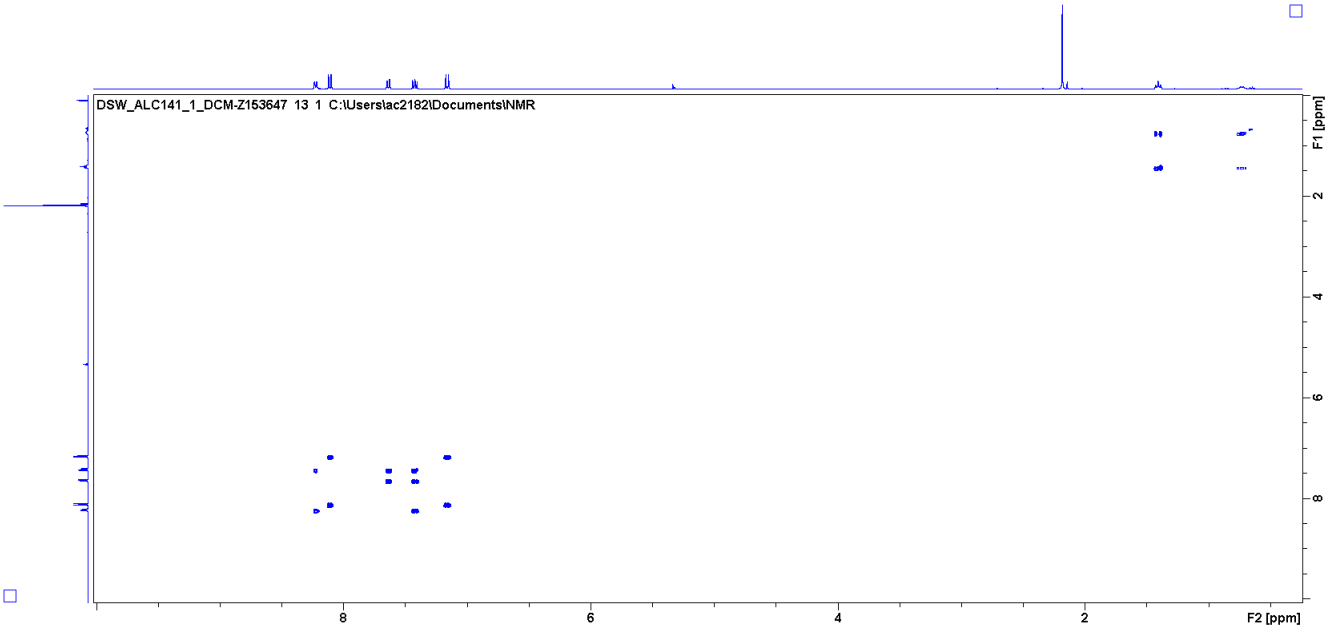

Figure S8: ^{1}H-^{1}H COSY NMR spectrum (25 °C, 400 MHz, CD_2Cl_2) of [{EtAl(2-Me-8-qy)$_3$}Li], [(**2**)Li].

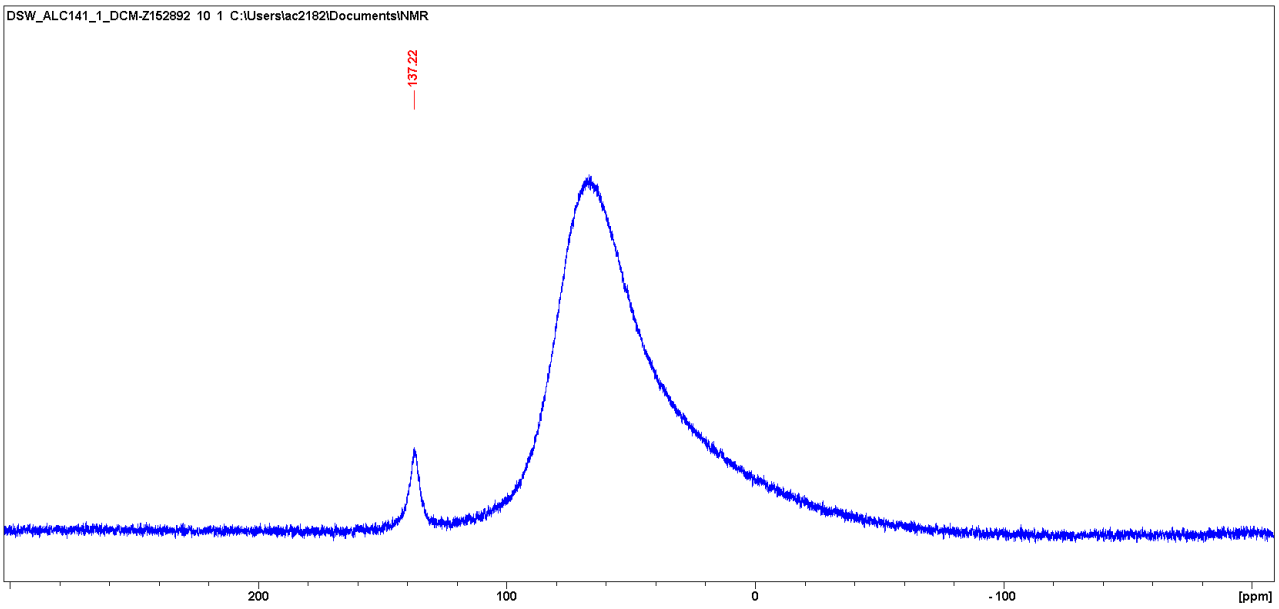

Figure S9: ^{27}Al NMR spectrum (25 °C, 104 MHz, CD_2Cl_2) of [{EtAl(2-Me-8-qy)$_3$}Li], [(**2**)Li].

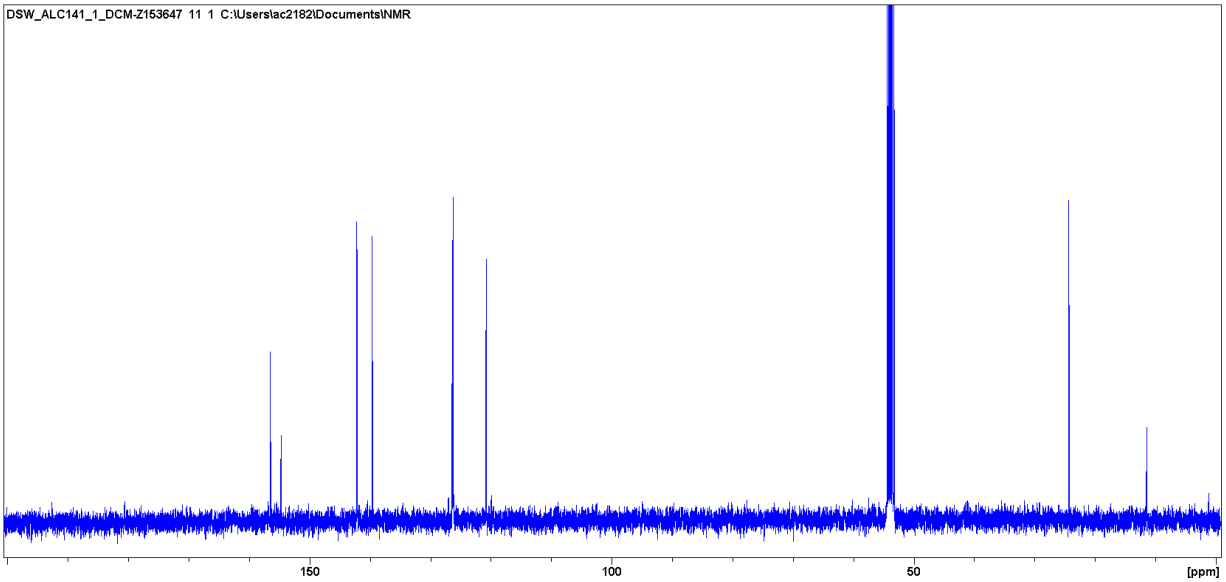

Figure S10: $^{13}C\{^{1}H\}$ NMR spectrum (25 °C, 101 MHz, CD_2Cl_2) of [{EtAl(2-Me-8-qy)$_3$}Li], [(**2**)Li]. C8 and the Et-CH_2 group are not observed.

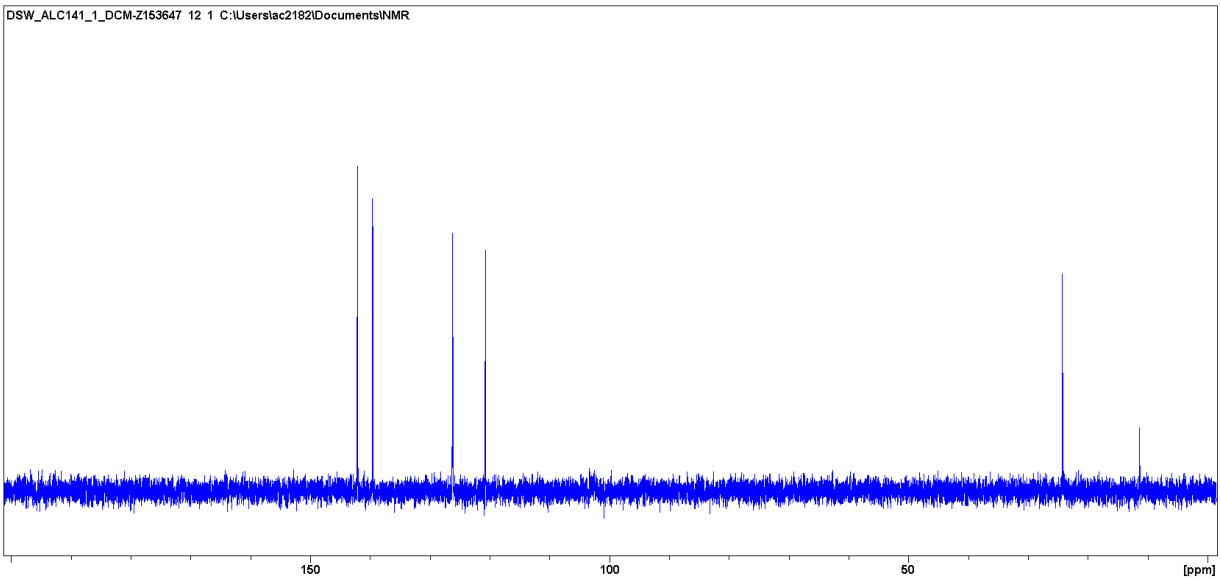

Figure S11: ^{13}C-DEPT NMR spectrum (25 °C, 101 MHz, CD_2Cl_2) of [{EtAl(2-Me-8-qy)$_3$}Li], [(**2**)Li].

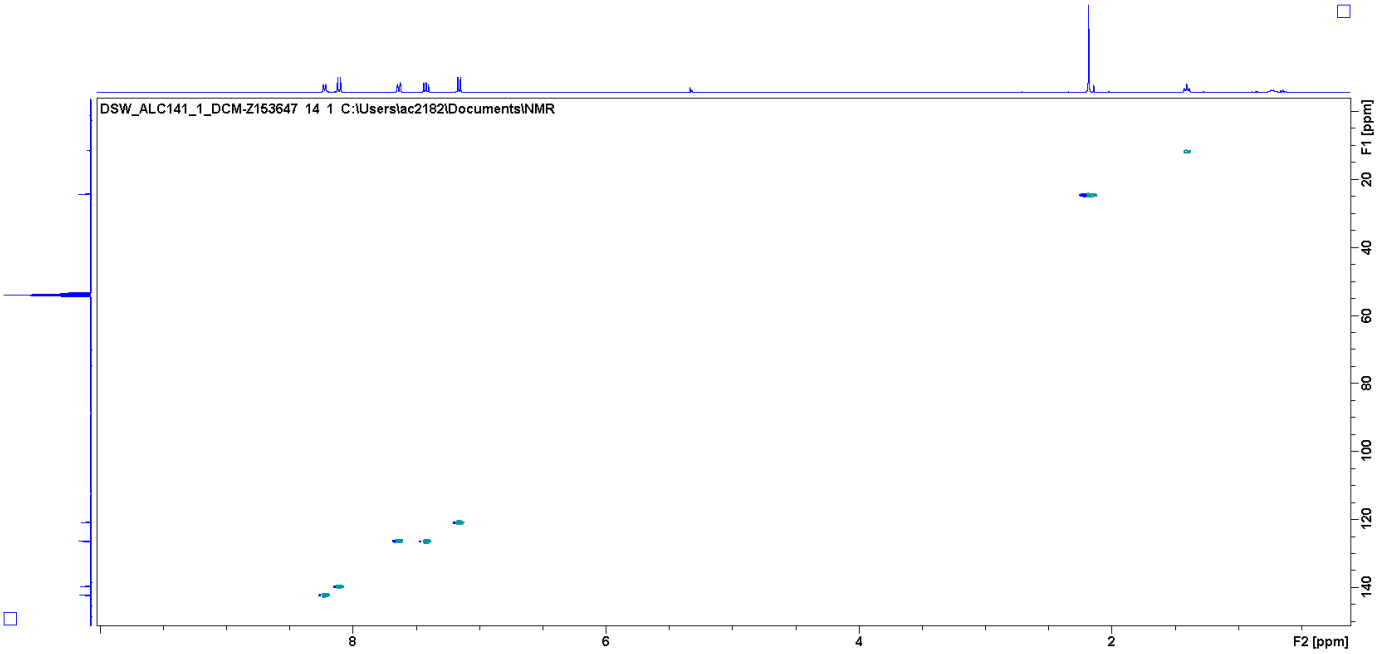

Figure S12: ^{1}H-^{13}C HSQC NMR spectrum (25 °C, CD_2Cl_2) of [{EtAl(2-Me-8-qy)$_3$}Li], [(**2**)Li].

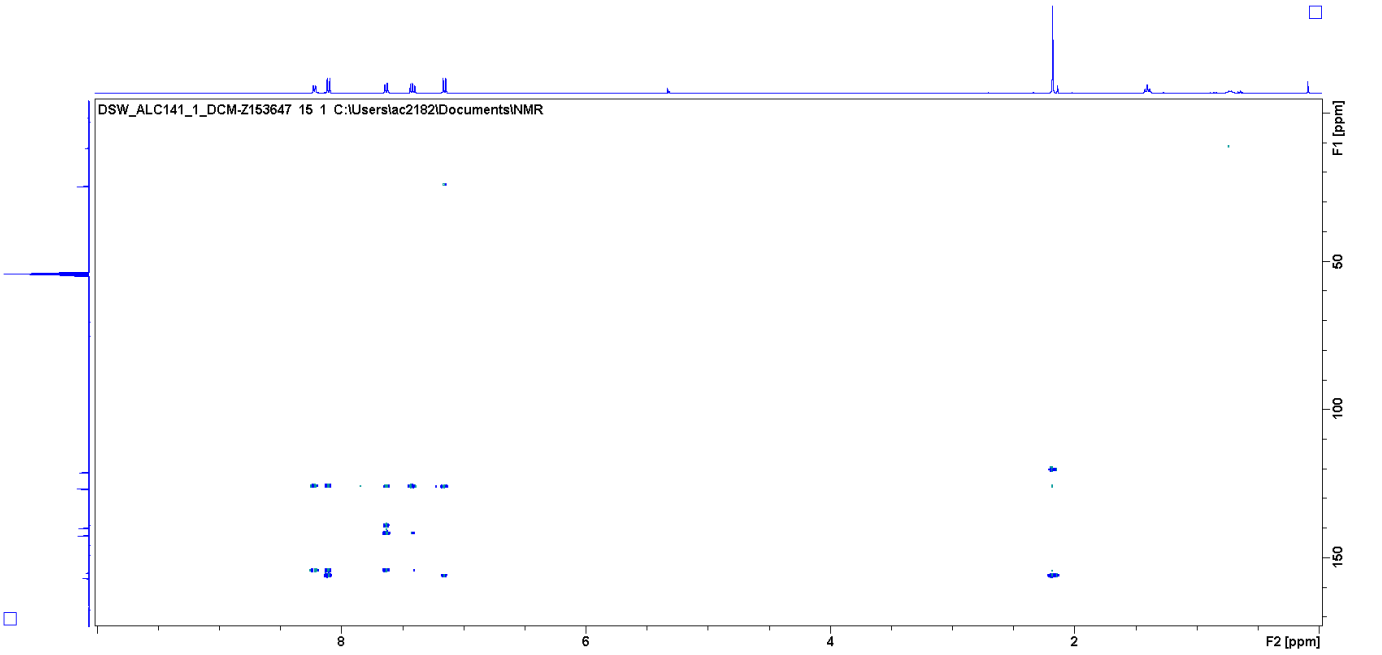

Figure S13: ^{1}H-^{13}C HMBC NMR spectrum (25 °C, CD_2Cl_2) of [{EtAl(2-Me-8-qy)$_3$Li], [(**2**)Li].

1.3 NMR spectra of [{$Me_2Al(2\text{-}Me\text{-}8\text{-}qy)_2$}Li(THF)], [(**3a**)Li(THF)]

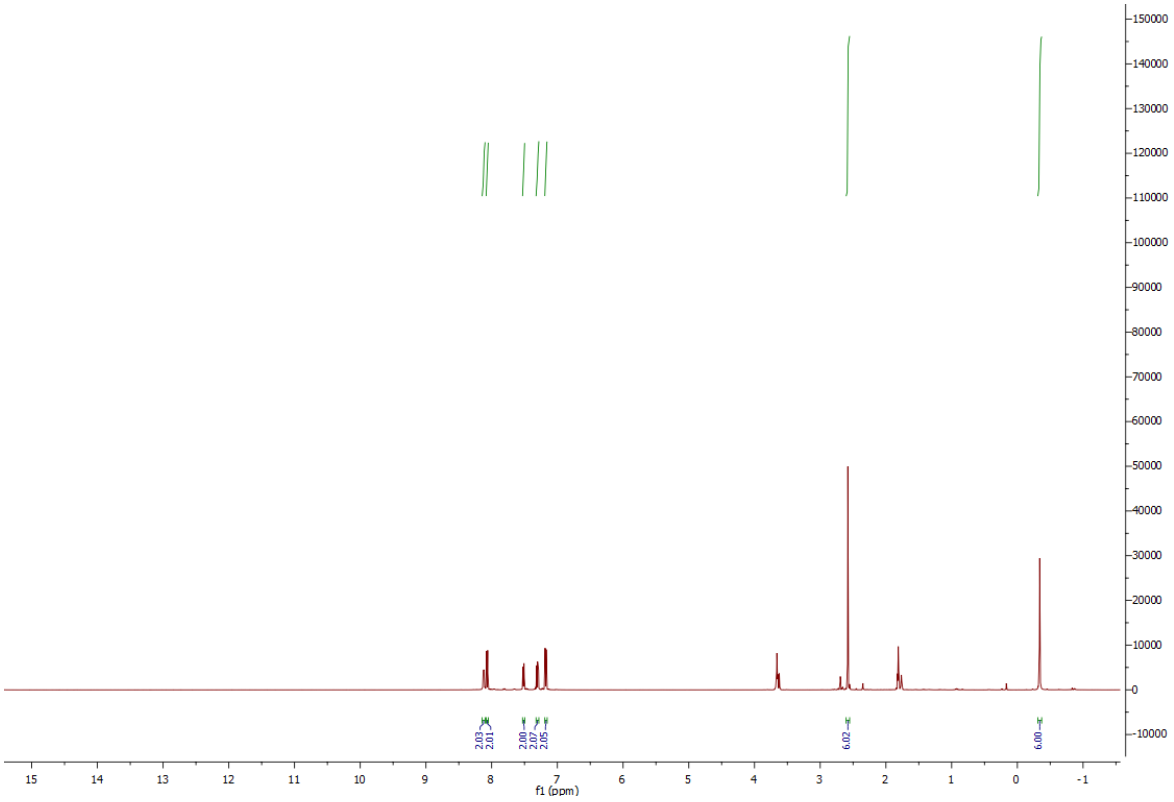

Figure S14: ^{1}H NMR spectrum (25 °C, 400 MHz, D_8-THF) of [{$Me_2Al(2\text{-}Me\text{-}8\text{-}qy)_2$}Li(THF)], [(**3a**)Li(THF)]. The spectrum shows that some of the THF has been removed during isolation under vacuum. This is consistent with elemental analysis of the complex when placed under vacuum for prolonged periods (which shows complete removal of the THF ligand).

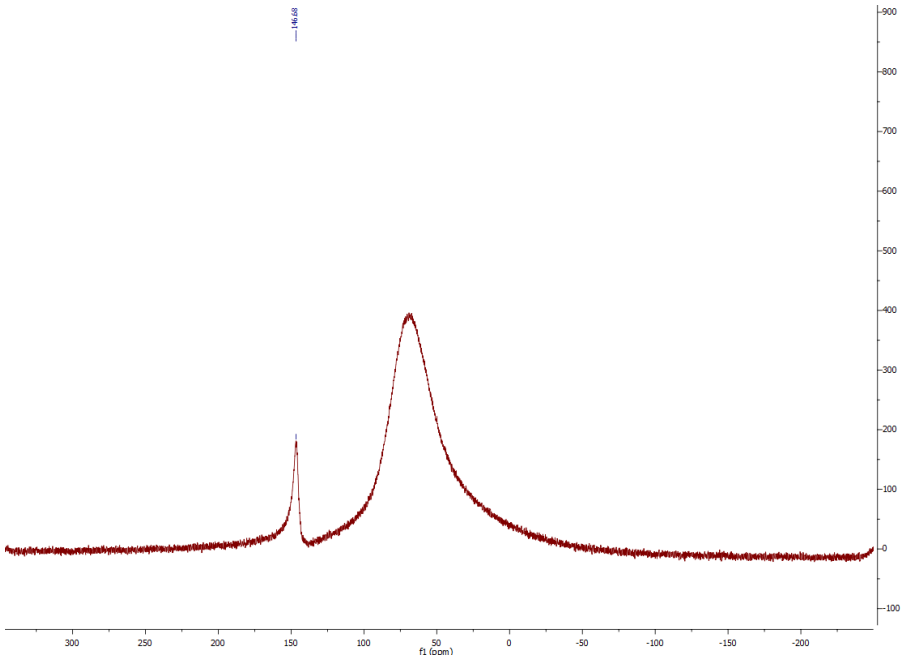

Figure S15: ^{27}Al NMR spectrum (25 °C, 104 MHz, D_8-THF) of [{$Me_2Al(2\text{-}Me\text{-}8\text{-}qy)_2$}Li(THF)], [(**3a**)Li(THF)].

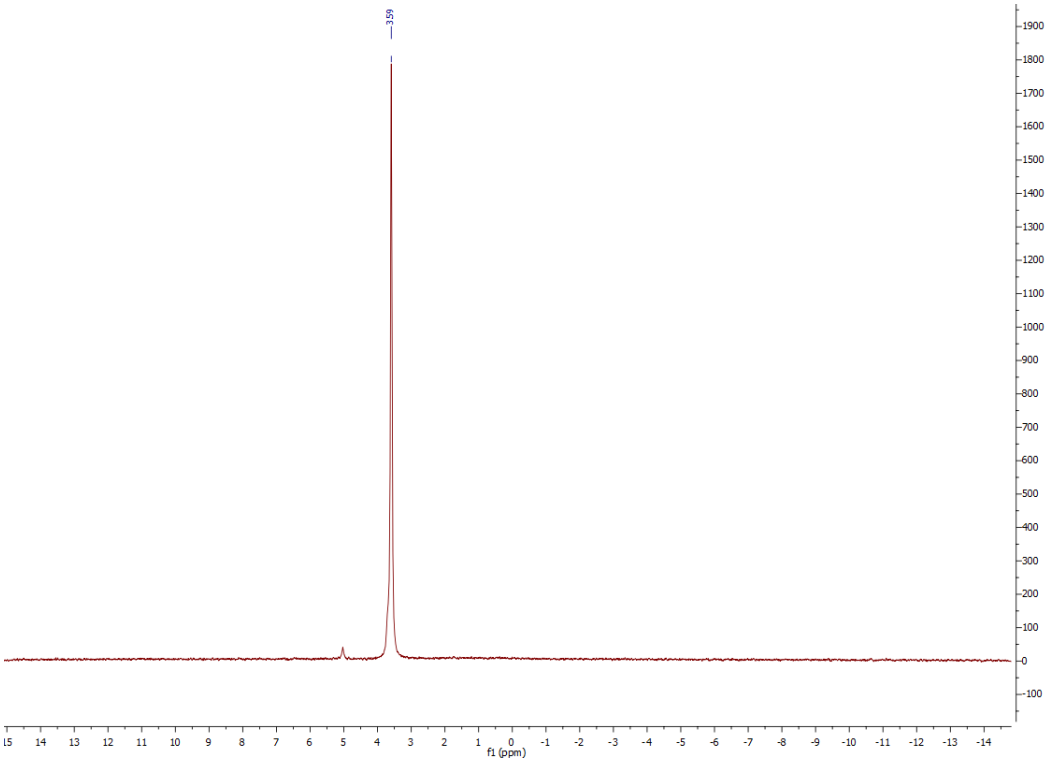

Figure S16: ^{7}Li NMR spectrum (25 °C, 155 MHz, D_8-THF) of [{Me_2Al(2-Me-8-qy)$_2$}Li(THF)], [(**3a**)Li(THF)].

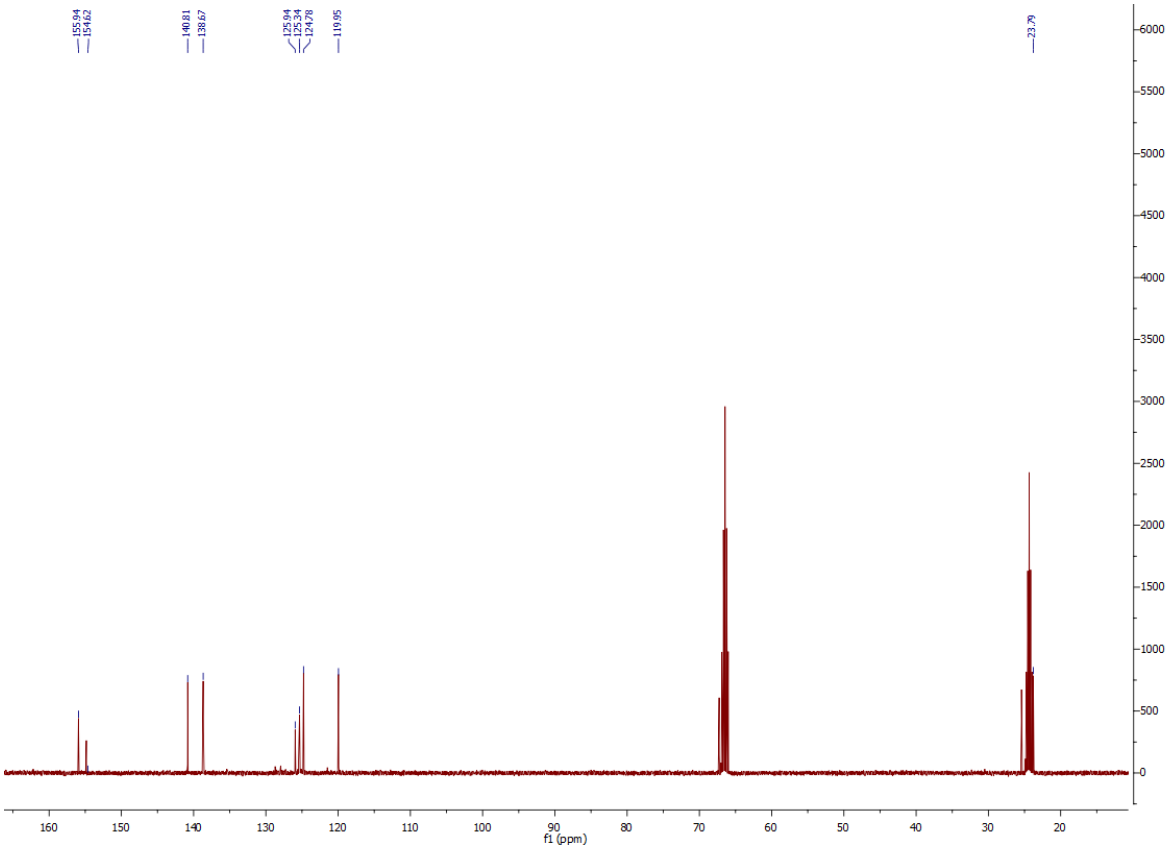

Figure S17: ^{13}C{^{1}H} NMR spectrum (25 °C, 101 MHz, D_8-THF) of [{Me_2Al(2-Me-8-qy)$_2$}Li(THF)], [(**3a**)Li(THF)] (the qy-Me resonance is partially obscured by the THF resonance at ca. 24 ppm, and C8 of the qy group and the Al-Me group were not observed).

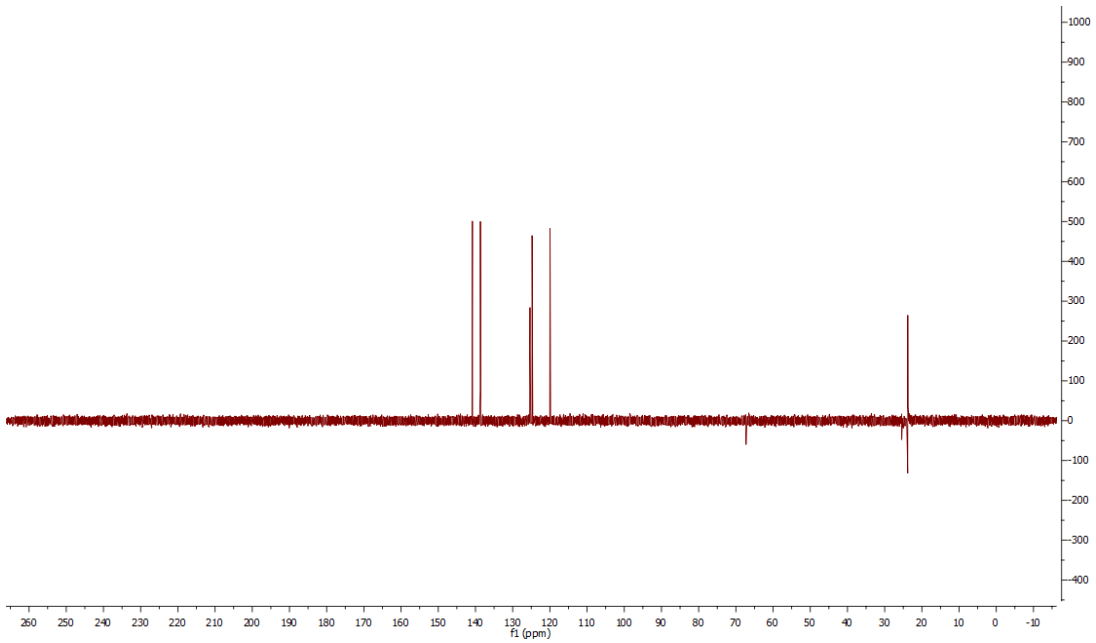

Figure S18: ^{13}C-DEPT NMR spectrum (25 °C, 101 MHZ, D_8-THF) of [{Me_2Al(2-Me-8-qy)$_2$}Li(THF)], [(**3a**)Li(THF)].

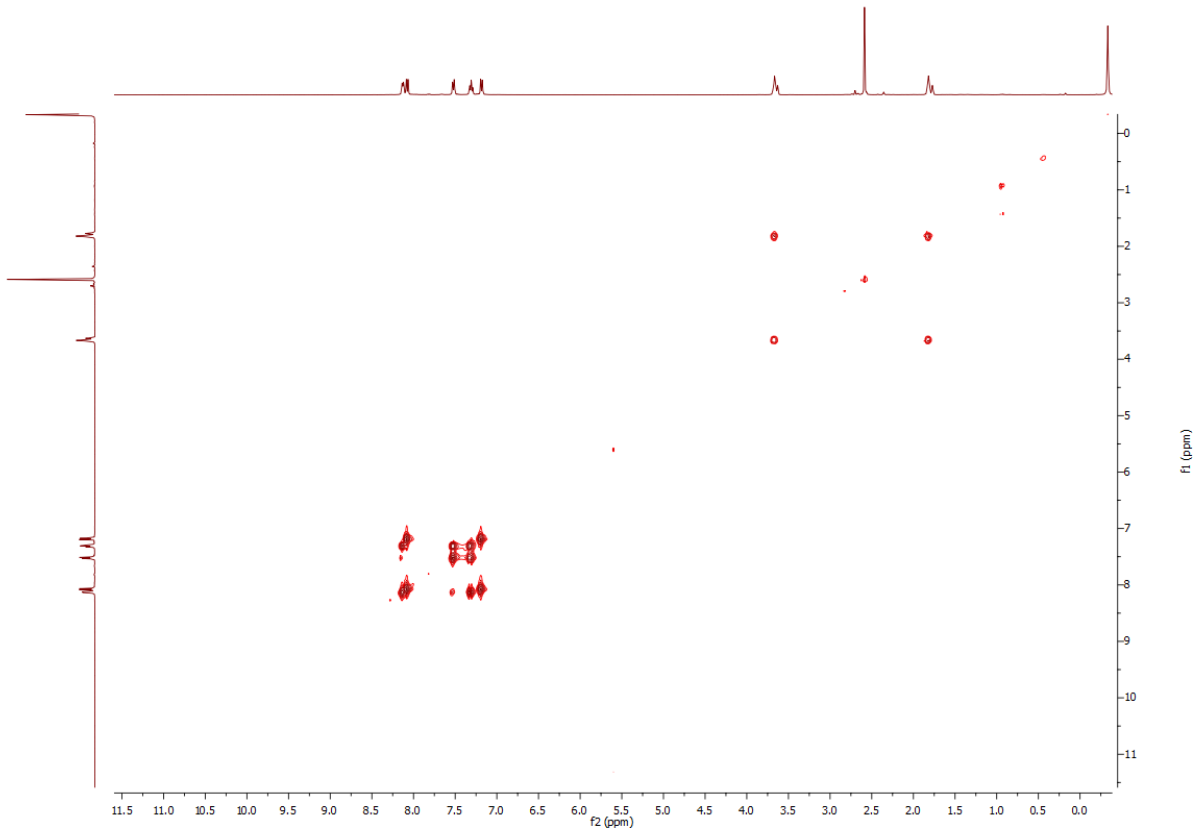

Figure S19: ^{1}H-^{1}H COSY NMR spectrum (25 °C, 400 MHZ, D_8-THF) of [{Me_2Al(2-Me-8-qy)$_2$}Li(THF)], [(**3a**)Li(THF)].

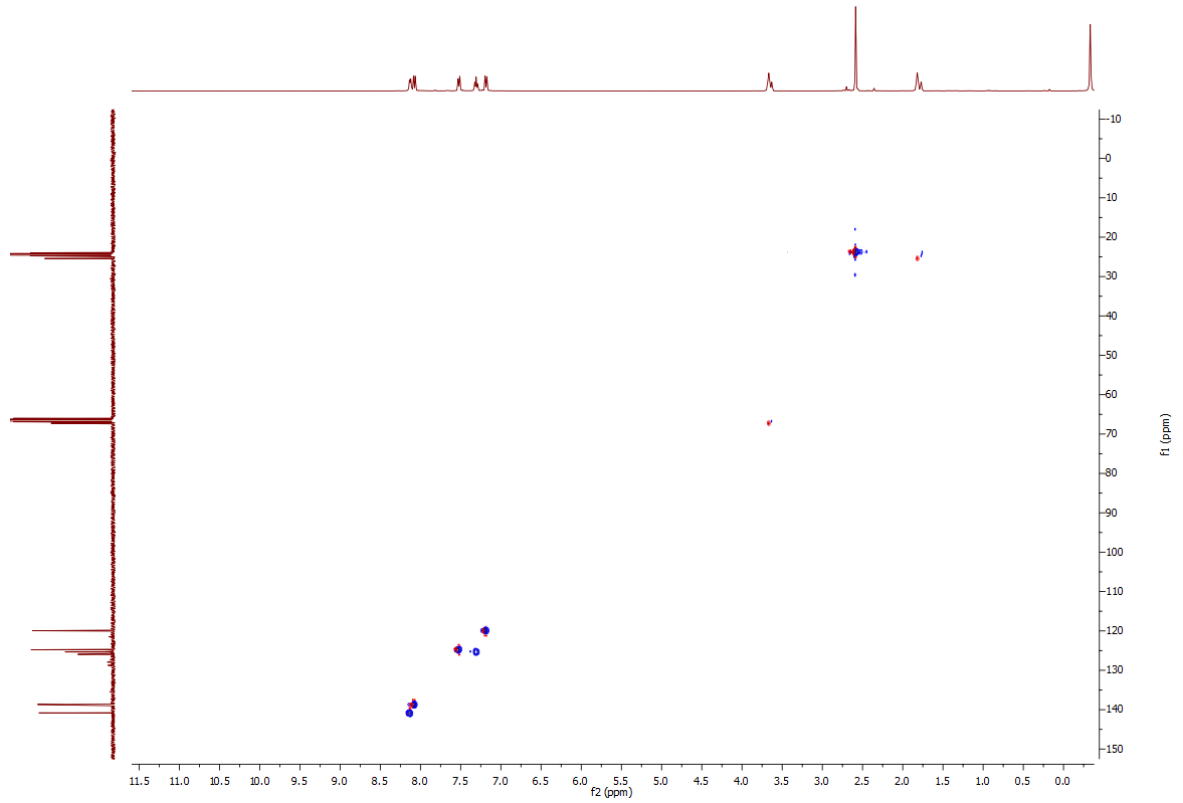

Figure S20: ^{1}H-^{13}C HSQC NMR spectrum (25 °C, D_8-THF) of [{$Me_2Al(2\text{-}Me\text{-}8\text{-}qy)_2$}Li(THF)], [(**3a**)Li(THF)].

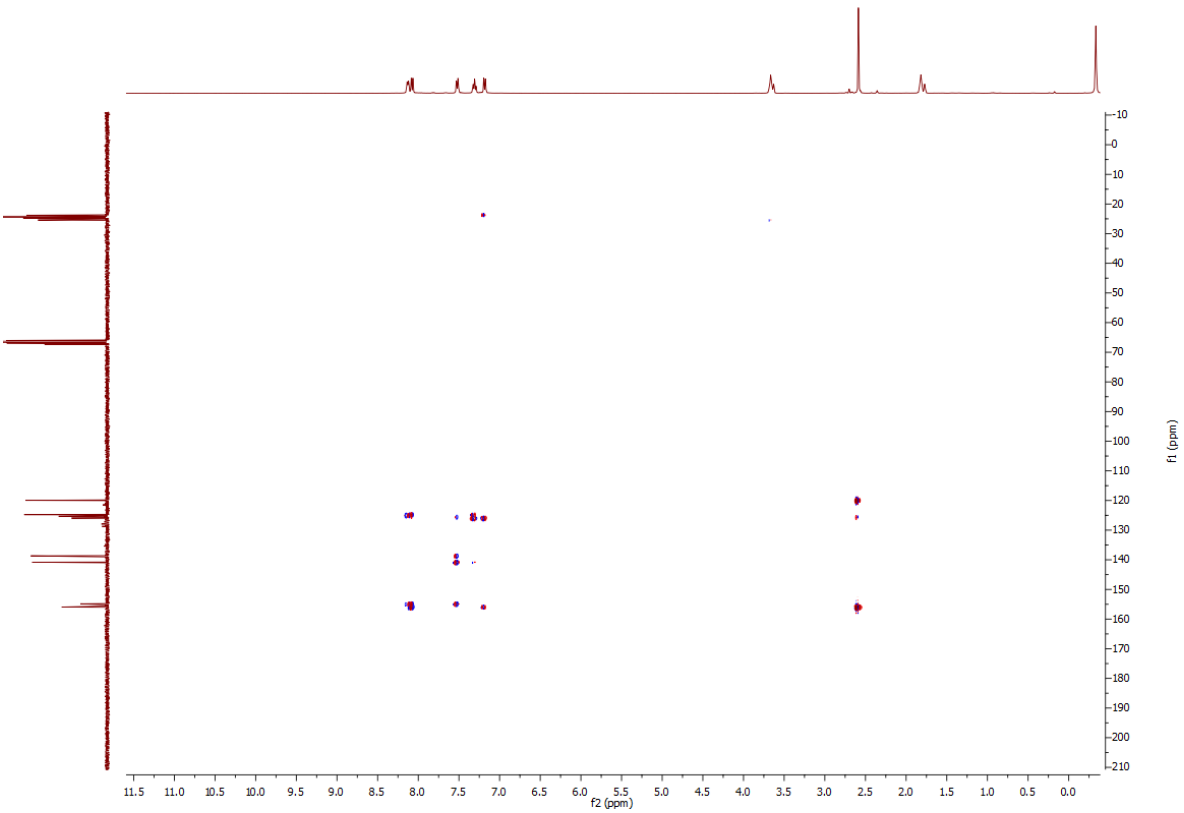

Figure S21: ^{1}H-^{13}C HMBC spectrum (25 °C, D_8-THF) of [{$Me_2Al(2\text{-}Me\text{-}8\text{-}qy)_2$}Li(THF)], [(**3a**)Li(THF)].

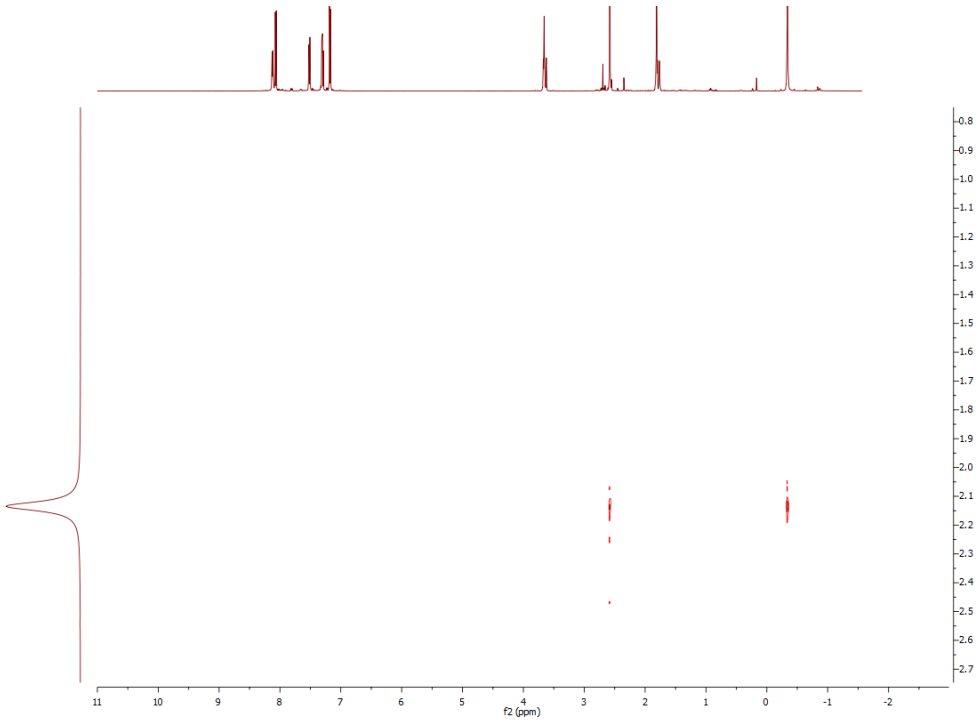

Figure S22: ^{7}Li-^{1}H HOSEY NMR spectrum (25 °C, D_8-THF) of [{Me_2Al(2-Me-8-qy)$_2$}]Li(THF)], [(**3a**)Li(THF)].

1.3 NMR spectra of [{Me_2Al(6-Me-2-py)$_2$}Li(THF)$_2$], [(4)Li(THF)$_2$]

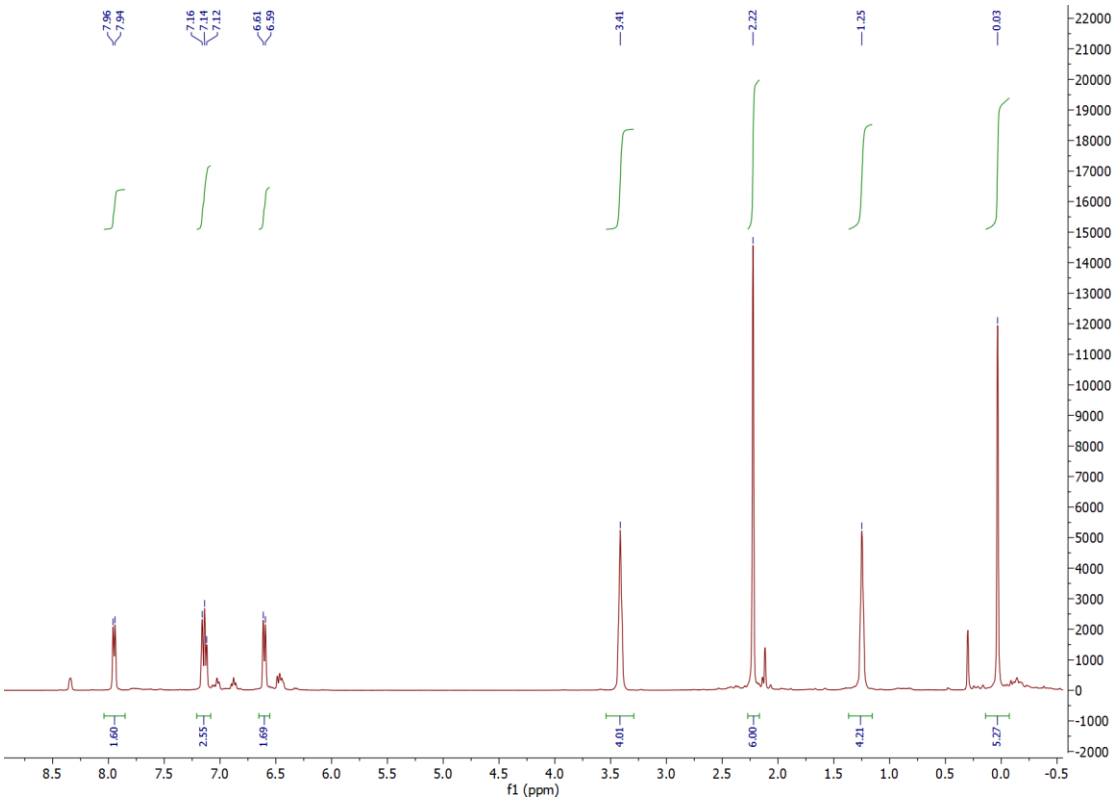

Figure S23: ^{1}H NMR spectrum (25 °C, 400 MHz, D_6-benzene) of [{Me_2Al(6-Me-2-py)$_2$}]Li(THF)$_2$], [(**4**)Li(THF)$_2$].

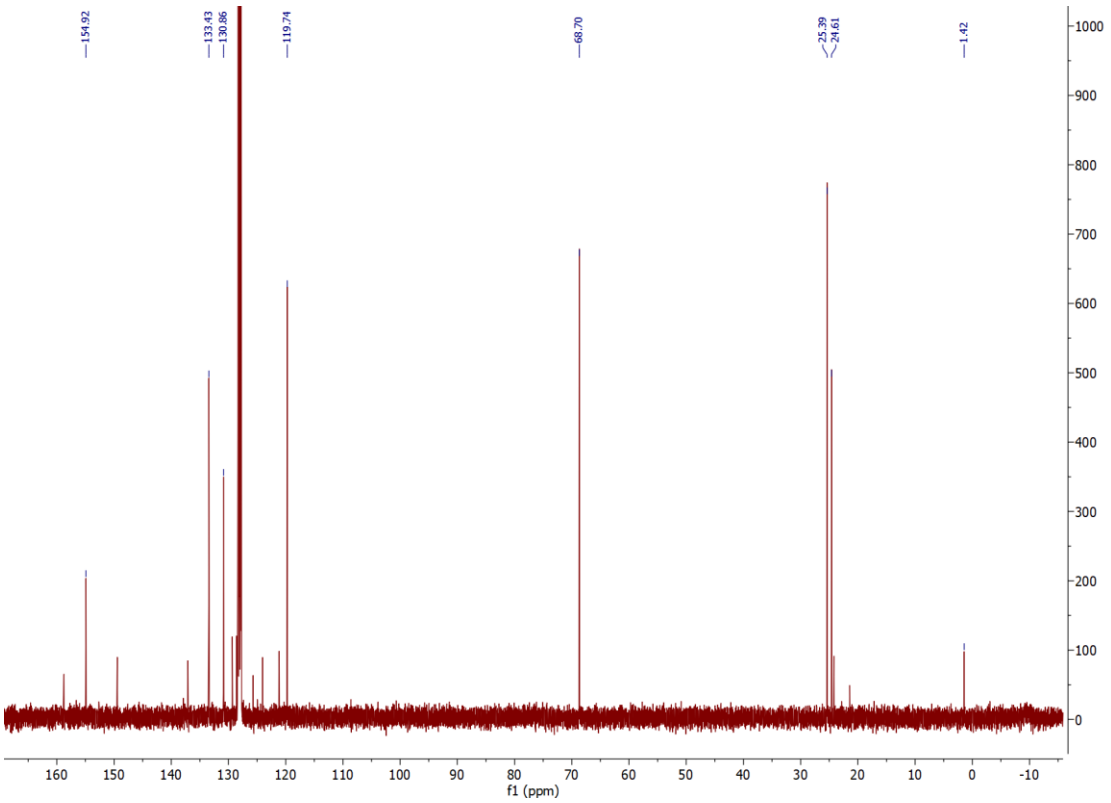

Figure S24: $^{13}C\{^{1}H\}$ NMR spectrum (25 °C, 101 MHz, D_6-benzene) of [{$Me_2Al(6\text{-}Me\text{-}2\text{-}py)_2$}$Li(THF)_2$], [(**4**)$Li(THF)_2$].

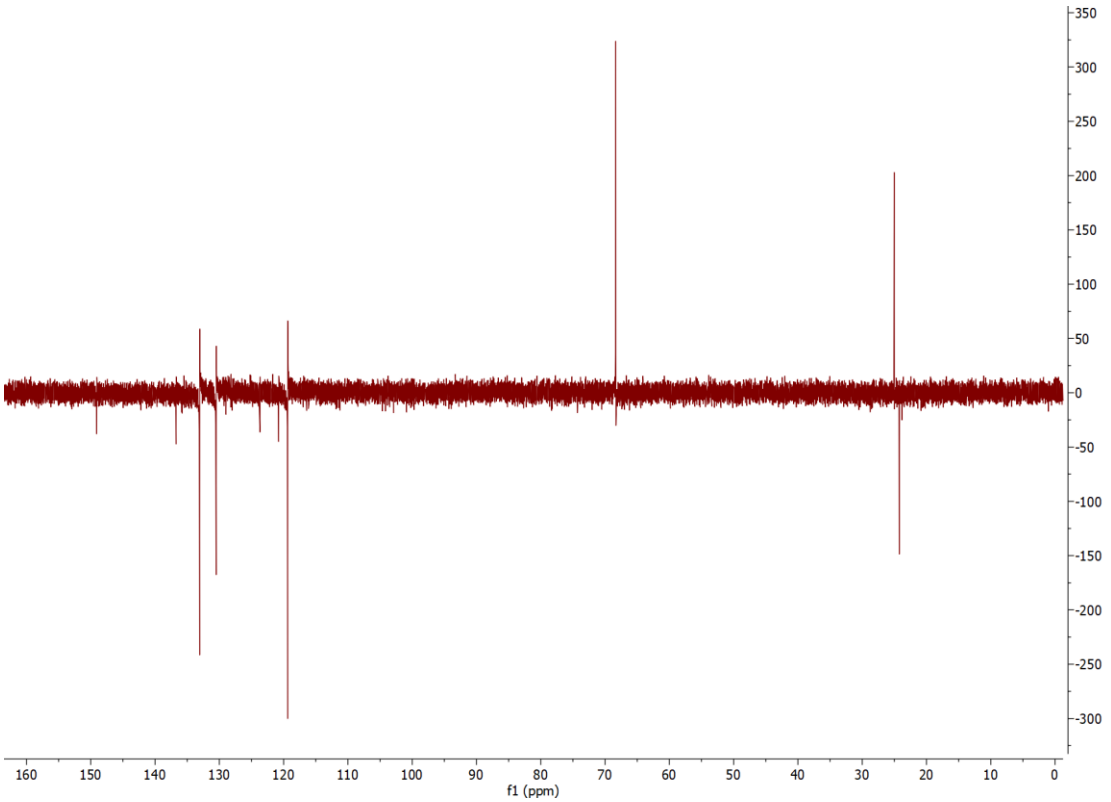

Figure S25: ^{13}C DEPT NMR spectrum (25 °C, 101 MHz, D_6-benzene) of [{$Me_2Al(6\text{-}Me\text{-}2\text{-}py)_2$}$Li(THF)_2$], [(**4**)$Li(THF)_2$].

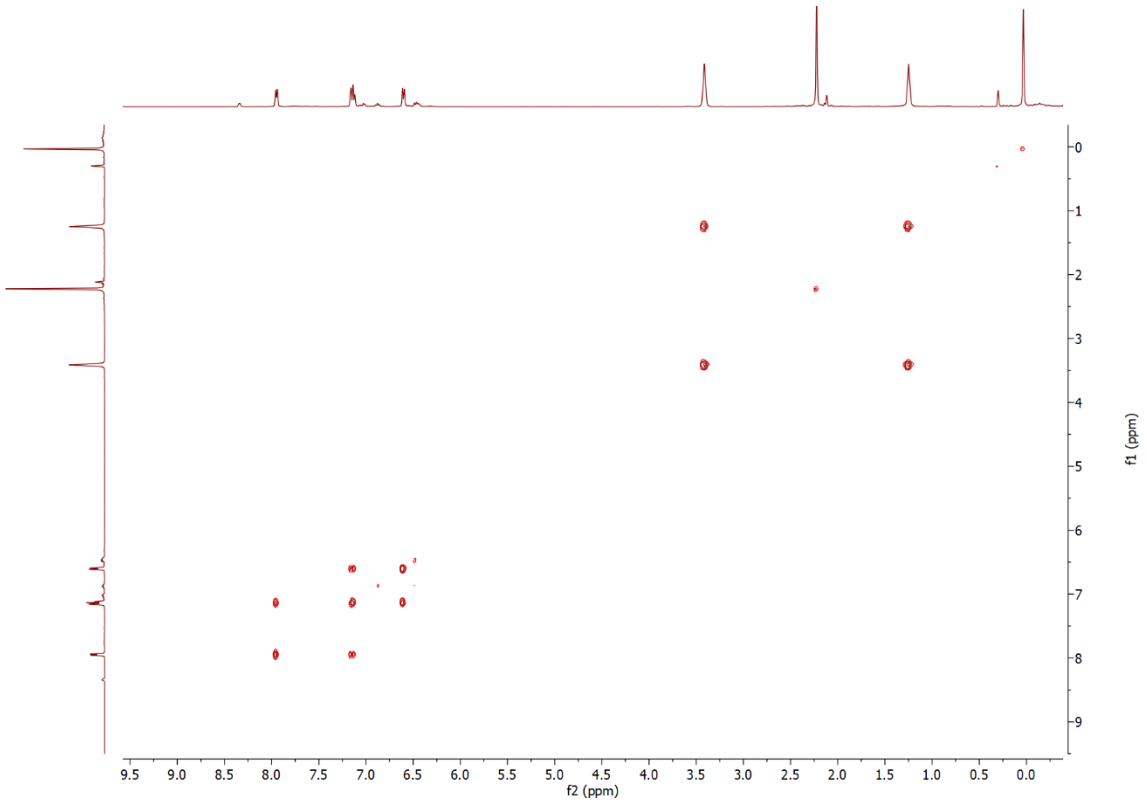

Figure S26: ^{1}H-^{1}H COSY NMR spectrum (25 °C, 400 MHz, D_6-benzene) of [{Me_2Al(6-Me-2-py)$_2$}Li(THF)$_2$], [(**4**)Li(THF)$_2$].

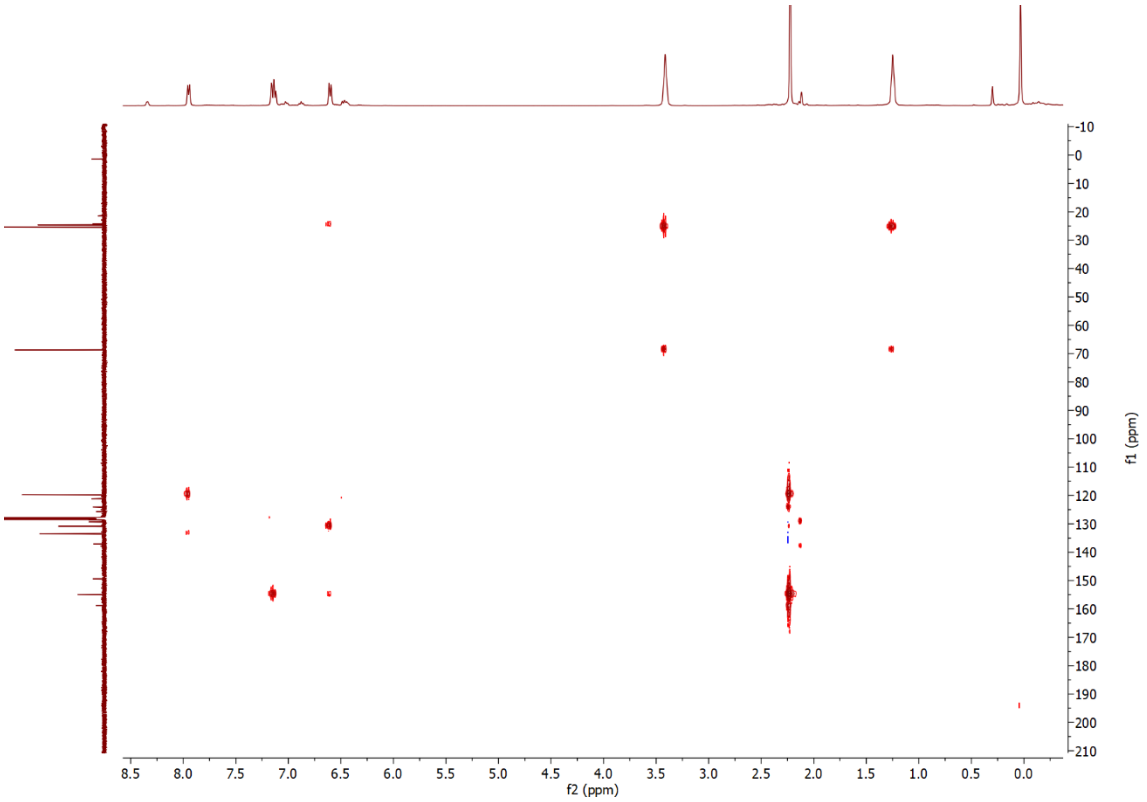

Figure S27: ^{1}H-^{13}C HMBC NMR spectrum (25 °C, D_6-benzene) of [{Me_2Al(6-Me-2-py)$_2$}Li(THF)$_2$], [(**4**)Li(THF)$_2$].

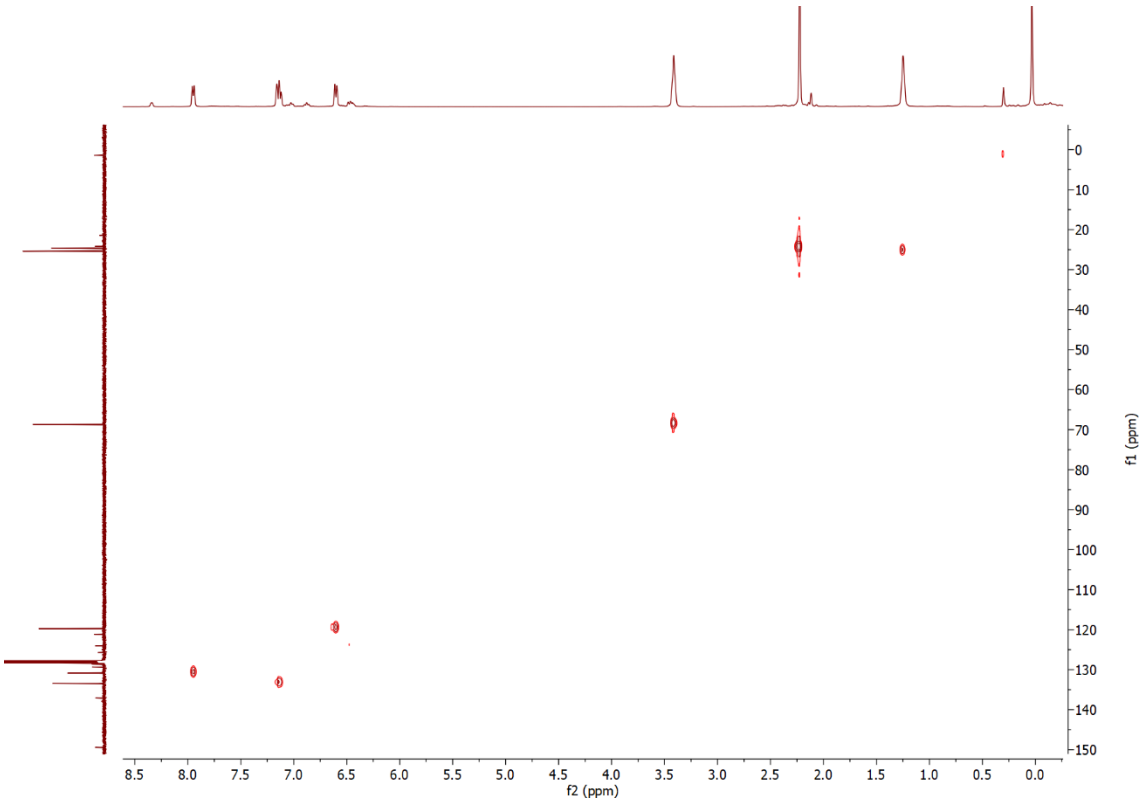

Figure S28: ^{1}H-^{13}C HSQC NMR spectrum (25 °C, D_6-benzene) of [{$Me_2Al(6\text{-}Me\text{-}2\text{-}py)_2$}$Li(THF)_2$], [(**4**)$Li(THF)_2$].

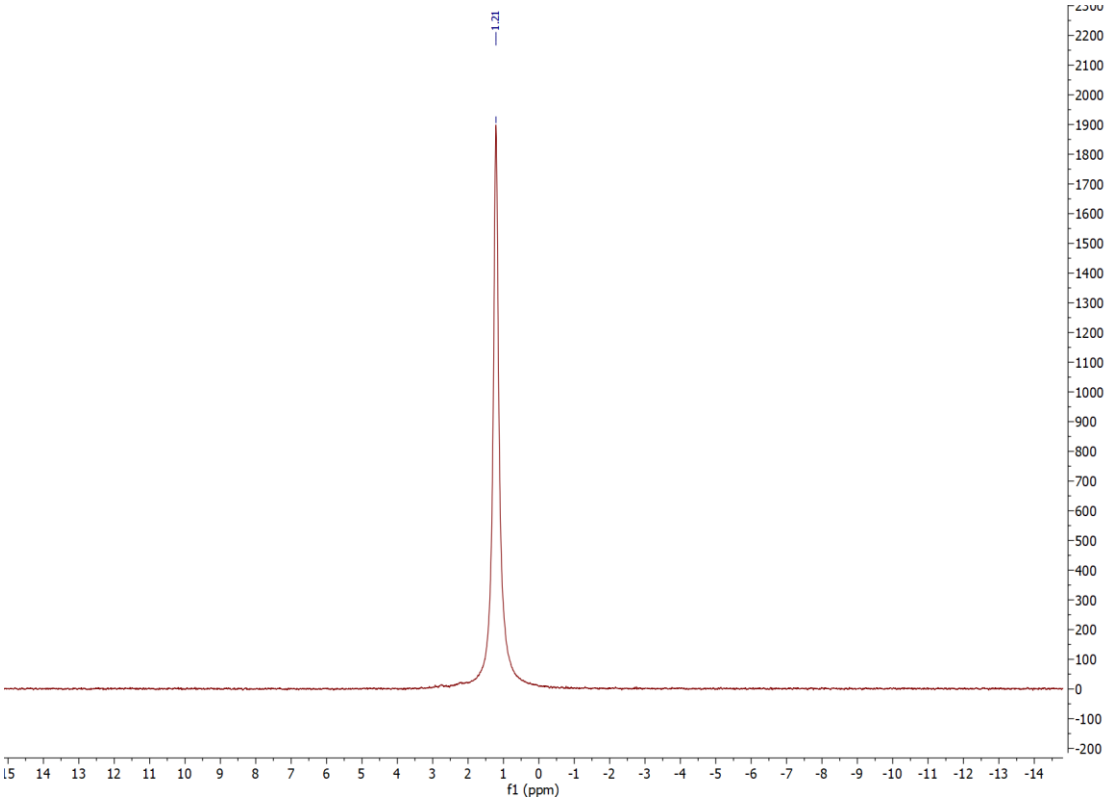

Figure S29: ^{7}Li NMR spectrum (25 °C, 156 MHz, D_8-THF) of [{$Me_2Al(6\text{-}Me\text{-}2\text{-}py)_2$}$Li(THF)_2$], [(**4**)$Li(THF)_2$].

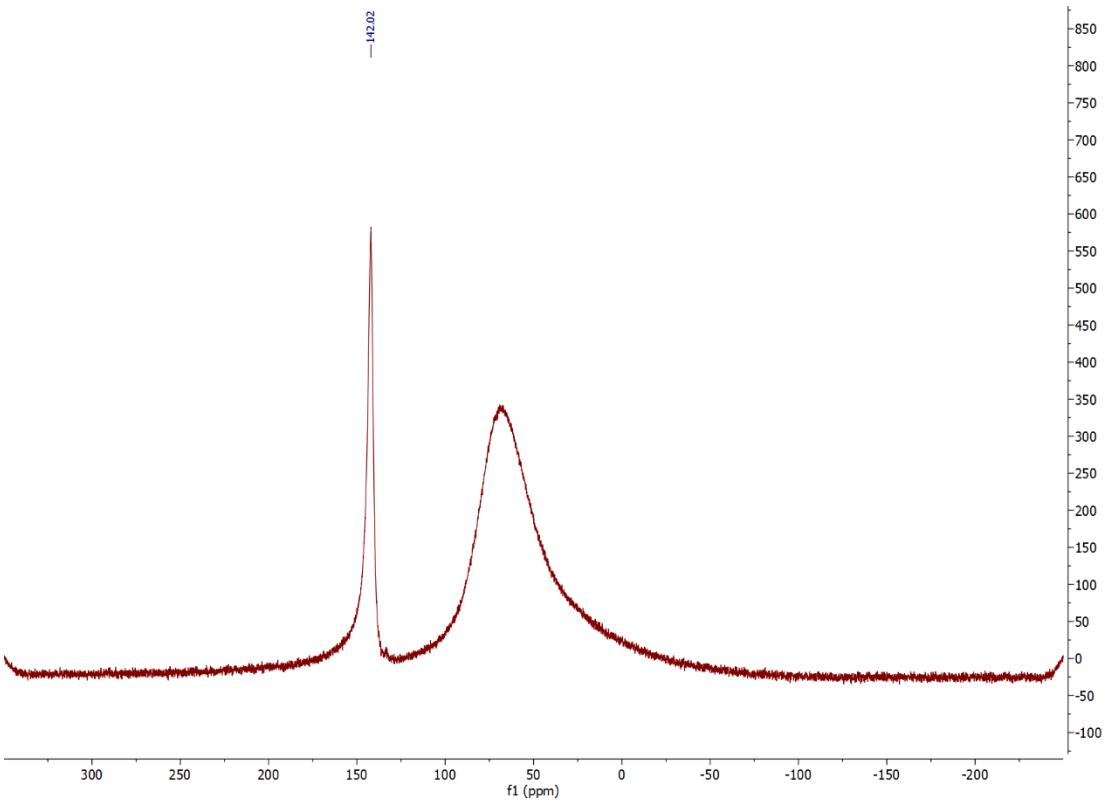

Figure S30: ^{27}Al NMR spectrum (25 °C, 104 MHz, D_8-THF) of [{Me_2Al(6-Me-2-py)$_2$}Li(THF)$_2$], [(**4**)Li(THF)$_2$].

1.4 NMR spectrum of 2,2′-biquinoline obtained from the crude reaction mixture from the synthesis of 1

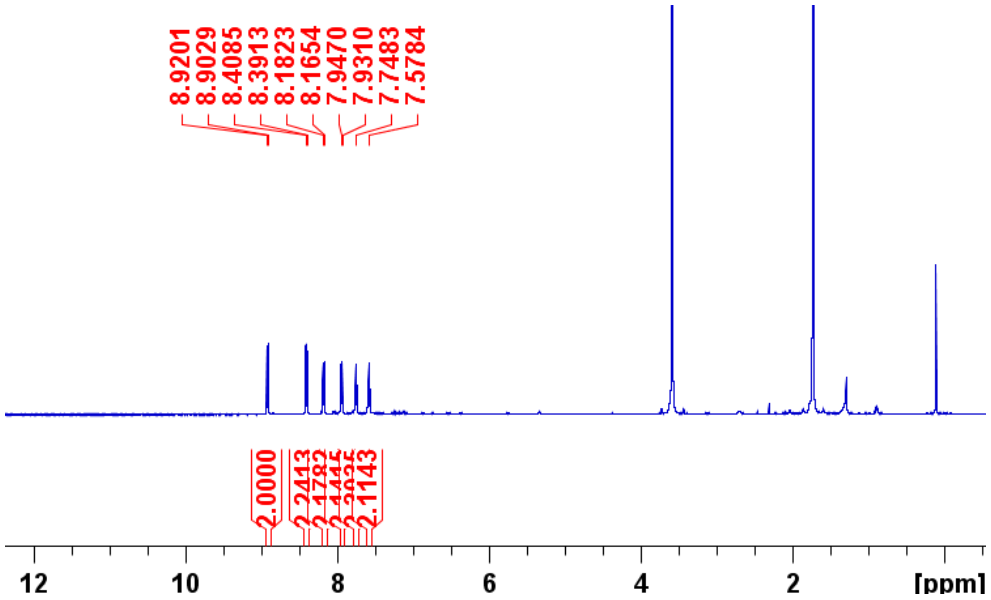

Figure S31: ^{1}H NMR spectrum (25 °C, 400 MHz, D_8-THF).

1.5 Mass spectrum of 2,2′-biquinoline obtained from crude reaction mixture from the synthesis of 1

Elemental Composition Report **Page 1**

Single Mass Analysis
Tolerance = 5.0 PPM / DBE: min = -1.5, max = 50.0
Element prediction: Off
Number of isotope peaks used for i-FIT = 3

Monoisotopic Mass, Even Electron Ions
6 formula(e) evaluated with 1 results within limits (up to 10 closest results for each mass)
Elements Used:
C: 3-18 H: 2-13 11B: 0-3 N: 1-2

DSW34250-ASAP
DSW34250-ASAP 947 (2.058) Cm (933:1058)

1: TOF MS ASAP+
2.12e+007

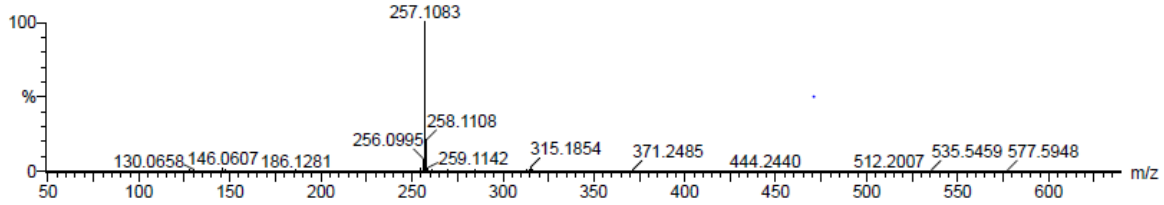

Minimum:				-1.5				
Maximum:		5.0	5.0	50.0				
Mass	Calc. Mass	mDa	PPM	DBE	i-FIT	Norm	Conf(%)	Formula
257.1083	257.1079	0.4	1.6	13.5	1063.7	n/a	n/a	C18 H13 N2

Figure S32: Mass spectrum, indicating the formation of 2,2′-biquinoline from reductive elimination from the anion **1** (m/z = 257.11 (observed), 257.11 (predicted) for (2,2′-biquinoline)H^+).

2. Synthesis of [{$Me_2Al(6\text{-}Me\text{-}2\text{-}py)_2$}$Li(THF)_2$], [(4)$Li(THF)_2$]

2-bromo-6-methylpyridine (0.5 ml, 4.4 mmol) was dissolved in THF (10 ml). ^{n}BuLi (1.6 M in hexanes, 2.75 ml, 4.4 mmol) was added dropwise to the solution at −78 °C, and the resulting dark red solution was stirred (2 h, −78 °C). Me_2AlCl (1.0 M in hexanes, 2.2 ml, 2.2 mmol) was added to the solution and stirred for 16 h. After warming up to room temperature overnight, solvent was removed *in vacuo* and the resulting orange oil was dissolved in 15 ml toluene to give a cloudy orange solution that was filtered through Celite. The solvent was removed to yield a dark orange solid (529 mg, 1.35 mmol, 61%). Crystals suitable for X-ray crystallographic analysis were grown from a solution of [(**4**)$Li(THF)_2$] in toluene at −20 °C.

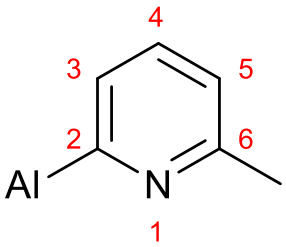

Figure S33: Numbering scheme used for NMR assignments.

^{1}H NMR (298 K, 400 MHz, D_6-benzene), δ [ppm] = 7.95 (d, *J* = 7.2 Hz, 2 H, C3-H), 7.14 (dd, *J* = 8.2, 8.2 Hz, 2 H, C4-H), 6.60 (d, *J* = 7.7 Hz, 2 H, C5-H), 3.41 (m, 4 H, -CH_2-O, THF), 2.22 (s, 6 H, py-Me), 1.25 (m, 4 H, -CH_2-, THF), 0.03 (s, 6 H, Al-Me).

^{13}C NMR (298 K, 101 MHz, D_6-benzene), δ [ppm] = 154.92 (C6), 133.43 (C4), 130.86 (C3), 119.74 (C5), 68.70 (-CH_2-O, THF), 25.39 (-CH_2-, THF), 24.61 (py-Me). C2 and Al-Me were not observed.

^{7}Li NMR (298 K, 156 MHz, D_8-THF), δ [ppm] = 1.21 (s).

^{27}Al NMR (298 K, 104 MHz, D_8-THF), δ [ppm] = 142.02 (s).

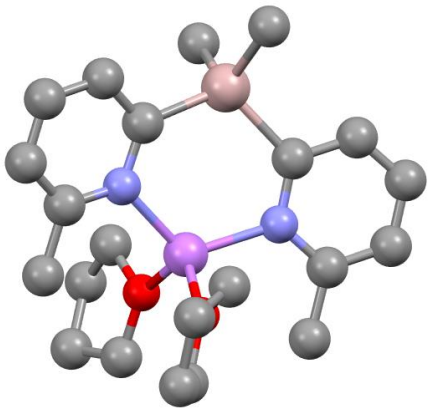

Figure S34: Solid-state structure of [(**4**)$Li(THF)_2$]. H-atoms omitted for clarity. Selected bond lengths (Å) and angles (°): C_{Me}-Al range 1.996(2)-2.000(2), C_{py}-Al range 2.028(2)-2.030(2), N-Li range 2.052(3)-2.068(3), Li-O range 1.971(3)-1.978(3), C_{py}-Al-C_{py} 113.70(8), C_{Me}-Al-C_{Me} 112.91(12), N-Li-N 118.36(15), O-Li-O 115.86(15). Colour code: C (grey), Al (pink), N (blue), Li (magenta), O (red).

3. Calculations

All calculations, except the NBO analyses, were carried out using the ORCA package (version: 4.2.1) in the gas phase.[1,2] For all ORCA calculations, atom-pairwise dispersion corrections with the Becke-Johnson damping scheme (D3BJ) were utilised.[3,4] Density fitting techniques, also called resolution-of-identity approximation (RI), were used for GGA calculations, whereas the RIJCOSX[5] approximation was used for hybrid calculations. Geometry optimisation, frequency analysis and single point calculations of [(**3a**)Li(THF)] were carried out at the TPSS,[6] def2-TZVP[7,8] level of theory. This functional was selected since the Li–H and Li–C bond lengths were represented best in comparison with the X-ray crystal structure. Additionally, the computational results were confirmed using the BP86[9–11] and B3LYP[12,13] functionals. NBO analyses[14,15] were computed using Gaussian 09 (Revision D.01).[16] The atoms in molecules method (AIMS) by Bader[17] was performed using the program package Multiwfn.[18] The strength of bonds, based on the electron density of the bond critical point, was estimated using the following equation: BE/kcal/mol = − 223.08 × ρBCP/a. u. + 0.7423.[19]

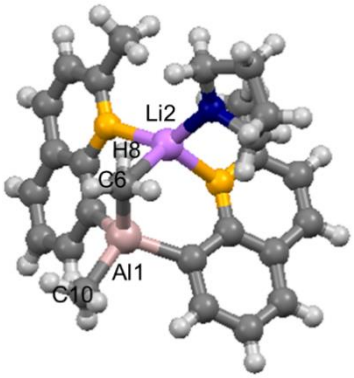

Figure S35: Atom numbering for the calculations.

Table S1: Loewdin population analyses.

Charges	
Al(1)	-0.046894
Li(2)	0.310678
C(6)	-0.45883
H(7)	0.141488
H(8)	0.120633
H(9)	0.121028
C(10)	-0.470837
H(11)	0.116535
H(12)	0.122179
H(13)	0.119725
Bond orders	
Li(2)-C(6)	0.1657
Li(2)-H(7)	-
Li(2)-H(8)	0.054
Li(2)-H(9)	-

Table S2: Wiberg bond order obtained by natural bond orbital analysis (NBO).

Wiberg bond order	
Al(1)-Li(2)	0.0188
Al(1)-C(6)	0.5628
Al(1)-C(10)	0.6164
Li(2)-C(6)	0.0268
Li(2)-H(7)	0.0016
Li(2)-H(8)	0.0087
Li(2)-H(9)	0.0023
C(6)-H(7)	0.931
C(6)-H(8)	0.9476
C(6)-H(9)	0.9474
Li(2)-C(10)	0.002
C(10)-H(11)	0.9496
C(10)-H(12)	0.9466
C(10)-H(13)	0.948

Table S3: Natural charges from natural population analysis.

Charges	
Al(1)	1.52165
Li(2)	0.84287
C(6)	-1.20734
H(7)	0.22604
H(8)	0.17788
H(9)	0.19662
C(10)	-1.19133
H(11)	0.19844
H(12)	0.20563
H(13)	0.20106

Table S4: Second order perturbation analyses. "BD" for 2-centre bond, "LP" for 1-centre valence lone pair, and "BD*" for 2-centre antibond.

Interactions	Stabilisation energy [kcal/mol]	Orbital description
LP*-Li(2)→BD*-C(6)-H(7)	3.20	LP*Li(2): s orbital BD*-C(6)-H(7): sp^3 hybrid orbital
LP*-Li(2)→BD*-C(6)-H(8)	4.20	LP*Li(2): s orbital BD*-C(6)-H(8): sp^3 hybrid orbital
LP*-Li(2)→BD*-C(6)-H(9)	1.32	LP*Li(2): s orbital BD*-C(6)-H(9): sp^3 hybrid orbital
BD-C(6)-H(8)→LP*-Li(2)	3.72	BD-C(6)-H(8): sp^3 hybrid orbital LP*Li(2): s orbital
LP-C(6)→LP*-Li(2)	2.49	LP-C(6): $sp^{3.6}$ hybrid orbital LP*Li(2): s orbital

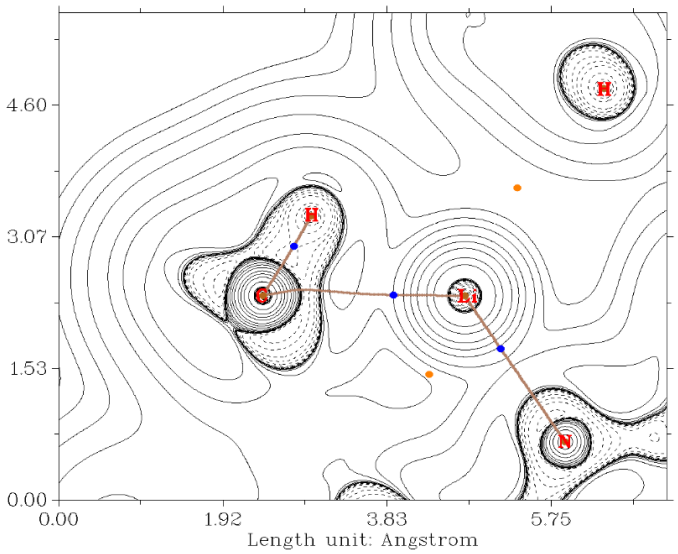

Figure S36: Graph of the Laplacian of the electron density of [(**3a**)Li(THF)]. Bond critical points and bond critical paths within the Li(2)-C(6)-H(8) plane.

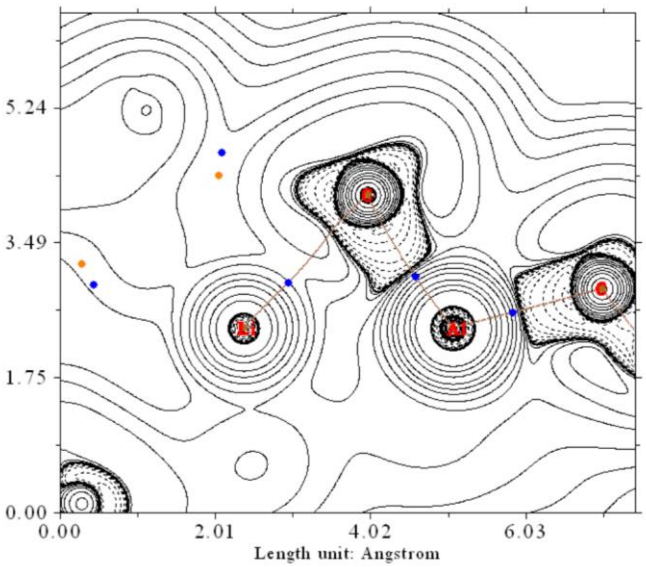

Figure S37: Graph of the Laplacian of the electron density of [(**3a**)Li(THF)]. Bond critical points and bond critical paths within the Al(1)-Li(2)-C(6) plane.

4. X-ray Crystallography

X-ray crystallographic data were collected using either a Nonius KappaCCD (sealed-tube MoKα) or Bruker D8-QUEST PHOTON-100 (Incoatec IμS Cu microsource) diffractometer. The temperature was held at 180(2) K using an Oxford Cryosystems N_2 cryostat. For the Nonius instrument, data integration and reduction were carried out using HKL DENZO/Scalepack and a multi-scan correction was applied using SORTAV. For the Bruker instrument, data integration and reduction were carried out with SAINT in the APEX3 software suite and a multi-scan correction was applied using SADABS. Structures were solved using SHELXT and refined using SHELXL.

Structure refinement was largely standard, with the following notes:

[{1Li}$_2$(μ-Br)]$^-$Li(THF)$_4^+$

- The structure contains toluene solvent molecules. One toluene molecule is clearly resolved and is refined in a standard way. It is situated on a crystallographic 2-fold axis, summing to two toluene molecules per unit cell. Additional voids exist in the structure in which individual toluene molecules could not be clearly resolved. SQUEEZE was applied to handle the electron density in these regions. In each void, SQUEEZE corrects for 48 electrons, appropriate for one toluene molecule (C_7H_8 = 50 electrons). Hence, a total of four toluene molecules per unit cell (one per formula unit) is included in the formula, formula weight and F(000).

[(1)Li(μ-Cl/Br)Li(THF)$_3$]

- The bridging atom is modelled as a mixture of Br and Cl. Both atoms were refined freely with anisotropic displacement parameters. The refined site occupancies are Cl : Br = 0.622(8) : 0.378(8). Attempts to refine with Cl or Br atoms only produced considerably higher R-factors.
- Two of the coordinated THF molecules are refined as disordered with two components. Bond distances, bond angles and anisotropic displacement parameters are restrained.
- The toluene molecule is refined as disordered over two orientations. Bond distances, angles and planarity are restrained, and isotropic displacement parameters are applied to all C atoms.
- Data are available only to 1.0 Å resolution, so the structure is of correspondingly lower precision. The main conclusions, namely the connectivity and Cl/Br disorder, are clear.

[(3a)Li(THF)]

- The toluene solvent molecule is positioned on a crystallographic inversion centre. The site occupancy factor for all atoms in the molecule is constrained to 0.5.
- In the final refinement, the H atoms on methyl group C(1) are placed geometrically, with rotation allowed around the local 3-fold axis (AFIX 137 in SHELXL). The resulting positions are in good agreement with positions indicated in the difference Fourier map (semi-transparent red spheres).

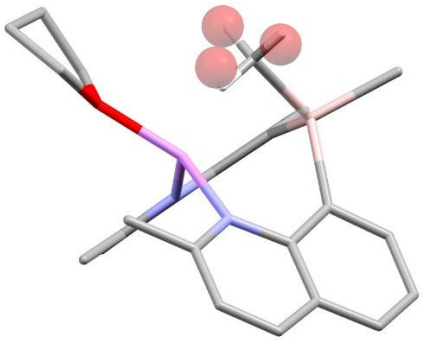

Table S5: Crystal Data and Refinements for Single-Crystal X-ray Structures.

	[(1)Li(μ-Cl/Br)Li(THF)$_3$]	**[{1Li}$_2$(μ-Br)]$^-$ Li(THF)$_4^+$**	**[(2)Li]**	**[(3a)Li(THF)]**	**[(4)Li(THF)$_2$]**	**5**
CCDC number	2096428	2096426	2096425	2096424	2097862	2096427
Cambridge data number	DW1435	DW_B2_0043	DW_B1_0313	DW_K1_0067	DW_B1_0400	DW_K3_0075
Chemical formula	$C_{48}H_{55}AlBr_{0.38}Cl_{0.62}Li_2N_3O_3$	$C_{81}H_{86}Al_2BrLi_3N_6O_4$ [**]	$C_{32}H_{29}AlLiN_3$	$C_{29.5}H_{34}AlLiN_2O$	$C_{22}H_{34}AlLiN_2O_2$	$C_{52}H_{58}Al_2Li_2N_4O_3$
Moiety formula	$C_{41}H_{47}AlBr_{0.38}Cl_{0.62}Li_2N_3O_3$, C_7H_8	$[C_{58}H_{46}Al_2BrLi_2N_6]^-$, $[C_{16}H_{32}LiO_4]^+$, C_7H_8 [**]	$C_{32}H_{29}AlLiN_3$	$C_{26}H_{30}AlLiN_2O$, 0.5(C_7H_8)	$C_{22}H_{34}AlLiN_2O_2$	$C_{48}H_{50}Al_2Li_2N_4O_2$, C_4H_8O
Formula weight	814.93	1362.24	489.50	466.50	392.43	854.86
Temperature / K	180(2)	180(2)	180(2)	180(2)	180(2)	180(2)
Crystal system	monoclinic	orthorhombic	monoclinic	triclinic	monoclinic	triclinic
Space group	$P2_1/n$	$P2_12_12$	$P2_1/n$	P–1	$P2_1/n$	P–1
a / Å	13.2730(3)	21.0518(6)	12.2250(9)	9.8424(3)	10.9054(4)	10.8075(2)
b / Å	17.3309(5)	21.3454(6)	13.9726(10)	10.1963(3)	15.1908(6)	13.5483(3)
c / Å	20.3751(4)	16.3309(5)	15.8078(12)	13.6820(5)	14.5647(5)	16.8949(4)
alpha / °	90	90	90	76.7685(10)	90	88.7384(10)
beta / °	90.3302(13)	90	91.136(5)	81.8527(11)	99.935(2)	80.4185(11)
gamma / °	90	90	90	89.3717(10)	90	70.9850(9)
Unit-cell volume / Å^3	4686.87(19)	7338.4(4)	2699.7(3)	1322.81(7)	2376.63(15)	2304.82(9)
Z	4	4	4	2	4	2
Calc. density / g cm^{-3}	1.155	1.233	1.204	1.171	1.097	1.232
F(000)	1723	2864	1032	498	848	908
Radiation type	MoKα	CuKα	CuKα	MoKα	CuKα	MoKα
Absorption coefficient / mm^{-1}	0.440	1.409	0.836	0.100	0.872	0.110
Crystal size / mm^3	0.23 x 0.23 x 0.18	0.18 x 0.14 x 0.11	0.21 x 0.13 x 0.06	0.35 x 0.20 x 0.18	0.22 x 0.14 x 0.04	0.18 x 0.12 x 0.05
2-Theta range / °	7.12-41.69	5.41-133.54	8.45-133.30	7.36-50.61	8.48-133.38	7.15-50.79
Completeness to max 2θ	0.973	0.998	0.997	0.985	0.997	0.983
No. of reflections measured	20738	84666	29543	11615	34188	21216

No. of independent reflections	4800	12996	4757	4751	4185	8324
R_{int}	0.0327	0.0647	0.1394	0.0465	0.0487	0.0501
No. parameters / restraints	538 / 162	847 / 60	339 / 0	336 / 0	257 / 0	574 / 0
Final R1 values ($I > 2\sigma(I)$)	0.0819	0.0682	0.0562	0.0582	0.0486	0.0555
Final $wR(F^2)$ values (all data)	0.0947	0.0848	0.1138	0.0957	0.0581	0.0924
Goodness-of-fit on F^2	1.034	1.041	1.021	1.034	1.071	1.018
Largest difference peak & hole / e $Å^{-3}$	0.545, -0.479	0.776, -1.256	0.296, -0.219	0.272, -0.237	0.329, -0.315	0.280, -0.308
Flack parameter		0.003(7)				

[**] There are four toluene molecule per unit cell, included in the formula, formula weight and F(000). Two toluene molecules are clearly resolved and refined in a conventional way. Two are poorly resolved and handled using SQUEEZE. SQUEEZE identifies two voids per unit cell and corrects for 48 electrons in each void. Toluene = C_7H_8 = 50 electrons.

5. References

1 F. Neese, *WIREs Comput. Mol. Sci.*, 2018, **8**, e1327.
2 F. Neese, *WIREs Comput. Mol. Sci.*, 2012, **2**, 73–78.
3 S. Grimme, S. Ehrlich and L. Goerigk, *J. Comp. Chem.*, 2011, **32**, 1456–1465.
4 S. Grimme, J. Antony, S. Ehrlich and H. Krieg, *J. Chem. Phys.*, 2010, **132**, 154104–154104.
5 F. Neese, F. Wennmohs, A. Hansen and U. Becker, *Chem. Phys.*, 2009, **356**, 98–109.
6 J. Tao, J. P. Perdew, V. N. Staroverov and G. E. Scuseria, *Phys. Rev. Lett.*, 2003, **91**, 146401-1-146401–4.
7 F. Weigend and R. Ahlrichs, *Phys. Chem. Chem. Phys.*, 2005, **7**, 3297–3305.
8 F. Weigend, *Phys. Chem. Chem. Phys.*, 2006, **8**, 1057–1065.
9 A. D. Becke, *Phys. Rev. A*, 1988, **38**, 3098–3100.
10 J. P. Perdew, *Phys. Rev. B*, 1986, **33**, 8822–8824.
11 J. P. Perdew, *Phys. Rev. B*, 1986, **34**, 7406.
12 A. D. Becke, *J. Chem. Phys.*, 1993, **98**, 5648–5652.
13 P. J. Stephens, F. J. Devlin, C. F. Chabalowski and M. J. Frisch, *J. Phys. Chem.*, 1994, **98**, 11623–11627.
14 E. D. Glendening, A. E. Reed, J. E. Carpenter and F. Weinhold, 1998.
15 A. E. Reed, L. A. Curtiss and F. Weinhold, *Chem. Rev.*, 1988, **88**, 899–926.
16 M. J. Frisch, G. W. Trucks, H. B. Schlegel, G. E. Scuseria, M. A. Robb, G. Cheeseman, J. R. Scalmani, V. Barone, B. Mennucci, G. A. Petersson, H. Nakatsuji, M. Caricato, X. Li, H. P. Hratchian, A. F. Izmaylov, J. Bloino, G. Zheng and D. J. Sonnenb, .
17 Atoms in Molecules - Richard F. W. Bader - Oxford University Press, https://global.oup.com/academic/product/atoms-in-molecules-9780198558651?cc=de&lang=en&, (accessed 25 February 2021).
18 T. Lu and F. Chen, *J. Comput. Chem.*, 2012, **33**, 580–592.
19 S. Emamian, T. Lu, H. Kruse and H. Emamian, *J. Comput. Chem.*, 2019, **40**, 2868–2881.